Eur. Phys. J. A (2024) 60:84
https://doi.org/10.1140/epja/s10050-024-01283-w

THE EUROPEAN PHYSICAL JOURNAL A

Regular Article - Theoretical Physics

Space-like electromagnetic form factors of lambda- and sigma-baryons from quark-diquark Faddeev equations

Langtian Liu[1,a], **Christian S. Fischer**[1,2,b]

[1] Institut für Theoretische Physik, Justus-Liebig-Universität Gießen, 35392 Gießen, Germany
[2] Helmholtz Forschungsakademie Hessen für FAIR (HFHF), GSI Helmholtzzentrum für Schwerionenforschung, Campus Gießen, 35392 Gießen, Germany

Received: 1 December 2023 / Accepted: 22 February 2024 / Published online: 9 April 2024

Communicated by Eulogio Oset

Abstract An important goal of ongoing and future experiments is to explore spectra and transition form factors of baryons with non-zero strangeness. Of particular interest is the transition form factor$\gamma^{(*)}\Sigma^0 \to \Lambda$ in the time-like momentum region that can be extracted from Dalitz decays. On the road towards a theoretical description of these form factors we extend a covariant dynamical quark-diquark model for the baryon Faddeev equation to the strange-quark sector. Based on an excellent description of the mass spectrum of selected baryon octet and decuplet states and reasonable results for the nucleon form factors we determine the elastic electromagnetic form factors of Λ and Σ^+, Σ^0, Σ^- hyperons in the space-like region as well as the ones for the octet transition $\gamma^{(*)}\Sigma^0 \to \Lambda$. We discuss qualitative and quantitative features of the diquark-quark picture and compare systematically with previous results from a three-body Faddeev approach and lattice data where available.

1 Introduction

The spectrum and the structure of baryons provide us with important opportunities to explore the strong interaction described by quantum chromodynamics (QCD). One of the most established probes of their internal structure are electromagnetic form factors (EMFFs) that allow to extract important global properties like charge radii and magnetic moments but also reveal detailed insights into the transition from perturbative to non-perturbative physics via their momentum dependence. While the electromagnetic form factors of baryons with zero net strangeness are very well explored, see e.g. [3–5] and references therein, single- and double-strange baryons received much less attention so far but are an important goal of ongoing and future experiments [1,2].

In general, it is very interesting to systematically compare properties and structure of baryons with different net strangeness. Taking all quantum fluctuations into account, the quark-gluon interaction becomes flavour-dependent and we may be able to extract valuable knowledge about the different roles of up/down and strange quarks inside baryons by comparing (transition) form factors and structure functions across the light and strange baryon multiplets.

On the experimental side, it is one of the primary goals of the HADES collaboration to extract information on the production and electromagnetic decays of hyperons in a FAIR-phase-0 experiment [2,6]. Here, the off-shell kinematics promises interesting insights into the time-like behaviour of the Σ to Λ transition. Theoretically, time-like form factors of hyperons have only been begun to be explored in recent years [7–12] with various approaches. The space-like region on the other hand is accessible with lattice QCD [13,14], has already been explored with functional methods (three-body Faddeev equations) [15,16] and can also be discussed by chiral perturbation theory (ChPT) [17], vector meson dominance models (VMD) [18–20] and light cone sum rules (LCSR) [21]. Furthermore, dispersion methods are very well suited to connect time-like and space-like physics in the small-Q^2 momentum region [22–25].

As explained in Ref. [26], the different yield rates of Λ and Σ hyperons in the experiments may indicate that internal diquark correlations in flavour space are also manifest in coordinate/momentum space. This suggests that a description in terms of a diquark-quark Faddeev equation may be a reasonable approach. The Poincaré covariant quark-diquark Faddeev equation can be derived from an exact equation for six-point functions using a separable expression for quark-quark T-matrices in terms of diquark propagators and Bethe–

[a] e-mail: Langtian.Liu@physik.uni-giessen.de
[b] e-mail: christian.fischer@theo.physik.uni-giessen.de (corresponding author)

Salpeter amplitudes [27,28]. In this approach, the diquarks are fully dynamical and have internal structure. The interaction with the third quark proceeds via attractive quark-exchange, which leads to the formation of baryon bound states and resonances. The diagrammatic expression of the equation is shown in Fig. 1 and explained in more detail below. There are good arguments both from theory and experiment for the existence of diquark correlations inside baryons, see e.g. Ref. [29] for a recent review.

Over time, the quark-diquark Faddeev equation approach has been employed successfully in the study of baryons [5,29], including mass spectra of octet and decuplet baryons [27,30–37], electromagnetic and axial form factors [38–49] as well as parton distribution functions [50–52]. Interestingly enough, when it comes to hyperon EMFFs no such investigation has been published so far to our knowledge. This work is intended as a starting point to fill this gap, since we believe that theoretical guidance from a variety of methods is beneficial for the interpretation of future experimental efforts in particular in the strange quark sector [2]. In this work, we therefore extend a model approach to the quark-diquark Faddeev equation including parametrizations of the strange quark resembling actual solutions of corresponding Dyson–Schwinger equations. An introduction to the quark-diquark Faddeev equation formalism of Λ and Σ is given in Sect. 2, whereas in Sect. 3 we discuss the necessary quark and diquark ingredients. We have solved the quark-diquark Faddeev equations for selected baryon octet and decuplet states and discuss our results in Sect. 4. The obtained mass spectrum is in very good agreement with the experimental values. In Sect. 5 we then discuss our results for the elastic EMFFs of Λ and Σ^+, Σ^0, Σ^- hyperons as well as the electromagnetic transition form factors of $\gamma^{(*)}\Sigma^0 \to \Lambda$ in the space-like momentum region and compare our results with that obtained from other theoretical methods as well as with experimental values (if possible). We summarize in Sect. 6.

Throughout this work, we assume isospin symmetry and perform our calculations in the Euclidean metric.

2 The quark-diquark Faddeev equation of Λ and Σ baryons

In the following we briefly recapitulate essential elements of the description of baryons using Faddeev equations. Much more details as well as guidance for the numerical treatment of this type of equations can be found e.g., in the review articles [5,53,54] and references therein.

Baryons obtain their quantum numbers from three valence quarks. Consequently the baryon wave function can be written as a spinor of rank three $\psi_{\alpha\beta\gamma}$ ($\alpha, \beta, \gamma = 1, 2, 3, 4$ are the Dirac spinor indexes). It is convenient to express this

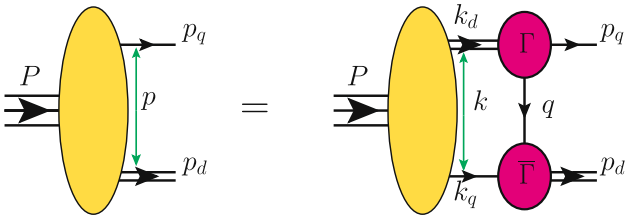

Fig. 1 The Feynman diagram of the quark-diquark Faddeev equation. The meaning of each quantity is explained in the context

rank three spinor in terms of a quark-diquark form, which is a general three-fermion wave function form [55].

In this work, we focus on baryons with two light and one strange quark, i.e. the Λ and Σ. Both have total spin $J = \frac{1}{2}$ and their quark-diquark amplitude can be written as

$$\psi = \psi_1 + \psi_2 + \psi_3. \tag{2.1}$$

Here, the subscript indicates the bystander quark which does not join to form a diquark. In the case of a bystander quark with index i the amplitude is given by a summation of all allowed diquark channels:

$$\psi_i(p, P) = \sum_a \left[\Gamma^a(l, p_d)D^a(p_d)\right]\left[\Phi_i^a(p, P)u(P)\right], \quad i = 1, 2, 3, \tag{2.2}$$

where $\Phi_i^a(p, P)$ is a matrix valued function in Dirac space corresponding to the diquark a. It can be expanded in an appropriate basis for different total spin and parity quantum numbers. Furthermore, $u(P)$ is the Dirac spinor of a baryon with mass M and satisfies the sum rule $\frac{1}{2M}u(P)\bar{u}(P) = \frac{iM+\gamma\cdot P}{2iM} \equiv \Lambda^+(P)$. The momentum P denotes the total momentum of the baryon and p is the relative momentum between bystander quark and diquark. The Bethe–Salpeter amplitude $\Gamma^a(l, p_d)$ of diquark a depends on the total diquark momentum p_d and the relative momentum l between two quarks inside the diquark. The quantity $D^a(p_d)$ is the diquark propagator with momentum p_d.

With given input, diquark propagators and Bethe–Salpeter amplitudes as well as quark propagators, the remaining unknown components in the baryon Bethe–Salpeter amplitude is determined by the quark-diquark Faddeev equation in the form

$$\Phi_i^a = \sum_b \sum_{j\neq i}^{3} \int \frac{d^4k}{(2\pi)^4} K_{ij}^{ab}(k, p, P)G_j^b(k, P)\Phi_j^b(k, P). \tag{2.3}$$

Here

$$G_j^b(k, P) = S_j(k_q)D^b(k_d), \tag{2.4}$$

is the combined quark and diquark propagator with quark momentum k_q and diquark momentum k_d, whereas

$$K_{ij}^{ab}(k,\,p,\,P) = \bar{\Gamma}_i^a(l_i,\,p_d)S^T(q)\Gamma_j^b(l_j,\,k_d), \tag{2.5}$$

is the quark exchange kernel. Here, $S^T(q)$ is the transposed quark propagator with momentum q. The Feynman diagram of this quark-diquark Faddeev equation is displayed in Fig. 1. For Λ and Σ with spin-1/2 and positive parity, the decomposition of matrix valued functions for scalar and axial-vector diquarks is shown in the appendix, Sec. A.1.

An additional element implicit in the equations above is the flavour part of the baryon amplitude. In terms of quark and diquark components the Λ and Σ baryons are composed as follows:

$$\begin{aligned}
\Lambda &\sim \begin{bmatrix} [ud]\,s \\ \frac{1}{\sqrt{2}}\left(-[ds]\,u - [su]\,d\right) \\ \frac{1}{\sqrt{2}}\left(-\{ds\}\,u + \{su\}\,d\right) \end{bmatrix}, \quad \Sigma^+ \sim \begin{bmatrix} -[su]\,u \\ \{uu\}\,s \\ -\{su\}\,u \end{bmatrix}, \\
\Sigma^- &\sim \begin{bmatrix} [ds]\,d \\ \{dd\}\,s \\ -\{ds\}\,d \end{bmatrix}, \\
\Sigma^0 &\sim \begin{bmatrix} \frac{1}{\sqrt{2}}\left([ds]\,u - [su]\,d\right) \\ \{ud\}\,s \\ \frac{1}{\sqrt{2}}\left(-\{ds\}\,u - \{su\}\,d\right) \end{bmatrix}, \quad \Xi^0 \sim \begin{bmatrix} -[su]\,s \\ \{su\}\,s \\ -\{ss\}\,u \end{bmatrix}, \\
\Xi^- &\sim \begin{bmatrix} [ds]\,s \\ \{ds\}\,s \\ -\{ss\}\,d \end{bmatrix},
\end{aligned} \tag{2.6}$$

where $[q_1q_2] = (q_1q_2 - q_2q_1)/\sqrt{2}$ denotes a flavour-antisymmetric scalar and $\{q_1q_2\} = (q_1q_2 + q_2q_1)/\sqrt{2}$ a flavour symmetric axialvector diquark.

3 Quarks and diquarks

In the past fifteen years, the quark-diquark Faddeev equation has been treated in several approaches with different philosophies. Starting from a truncation of the quark-gluon interaction, one can solve the Dyson–Schwinger equation of the quark propagator in the complex momentum space, subsequently solve the corresponding Bethe–Salpeter equations for all diquarks needed in a given truncation and then use this input in the quark-diquark Faddeev equation to determine the baryon amplitudes. This program has been carried out with contact interactions between quarks as well as in rainbow-ladder type truncations using models for the effective quark-gluon coupling, see e.g. [5,53,56] for overviews. The second, and admittedly much more ad hoc method is to use model functions representing the most important properties of the quark and diquark propagators as well as their wave functions. This type of modelling has been pioneered in [27,30] and is still in use today (see e.g [48,49] and Refs. therein) due to its simplicity.

The present work is part of a research program that ultimately aims at calculating transition form factors in the time-like region. Since simplicity is vital in first exploratory studies we resort to the diquark-quark model approach and postpone more fundamental rainbow-ladder type calculations to future works.

We therefore use parametrized quarks and diquarks. For u, d quarks, we adopted the original forms and parameters which have been shown to describe the nucleons and Δ-baryons well [38,43,49,57]. The quark propagator has the form

$$S(p) = -i\not{p}\sigma_v(p^2) + \sigma_s(p^2)\,, \quad \sigma_v = \frac{\bar{\sigma_v}}{\lambda^2}\,, \quad \sigma_s = \frac{\bar{\sigma_s}}{\lambda}\,, \tag{3.1}$$

with propagator functions σ_v and σ_s and

$$\begin{aligned}
\bar{\sigma_v}(x) &= \frac{1}{x+\bar{m}^2}\left[1 - \mathcal{F}\left(2(x+\bar{m}^2)\right)\right], \\
\mathcal{F}(x) &= \frac{1-\exp[-x]}{x}\,,
\end{aligned} \tag{3.2}$$

$$\begin{aligned}
\bar{\sigma_s}(x) &= 2\bar{m}\mathcal{F}\left(2(x+\bar{m}^2)\right) \\
&\quad + \mathcal{F}(b_1x)\mathcal{F}(b_3x)\left[b_0 + b_2\mathcal{F}(\epsilon x)\right], \quad x = \frac{p^2}{\lambda^2}\,,
\end{aligned} \tag{3.3}$$

and the parameters are shown in Table 1.

For the s quark, we assume a similar functional form but adapt the parameters by fitting to an explicit solution of the strange quark Dyson–Schwinger equation obtained in the truncation of Ref. [58]. Its parameters are also shown in Table 1.

Defining the inverse quark propagator as

$$S^{-1}(p) = i\not{p}A(p^2) + B(p^2) = A(p^2)\left(i\not{p} + M(p^2)\right), \tag{3.4}$$

the dressing functions A, B, M of u, d and s quarks are depicted in Fig. 2 as a function of space-like momentum p^2. One clearly distinguishes the large momentum behaviour of the dressing functions ('current quarks') from the small momentum region, where dynamical chiral symmetry breaking and the associated quark mass generation sets in. At zero momenta one may read off 'constituent quark' masses of the order of 400 MeV for the up/down quarks and 700 MeV for the strange quark mass.

Table 1 The parameters of our representations of the u, d and s quark propagators, Eqs. 3.1–3.3

$\lambda_{u,d}$	$\bar{m}_{u,d}$	$b_0^{u,d}$	$b_1^{u,d}$	$b_2^{u,d}$	$b_3^{u,d}$	ε
0.566	0.00897	0.131	2.90	0.603	0.185	0.0001
λ_s	$\bar{m}_s$	b_0^s	b_1^s	b_2^s	b_3^s	
0.817556	0.223	0.198323	1.19203	0.202049	1.19204	

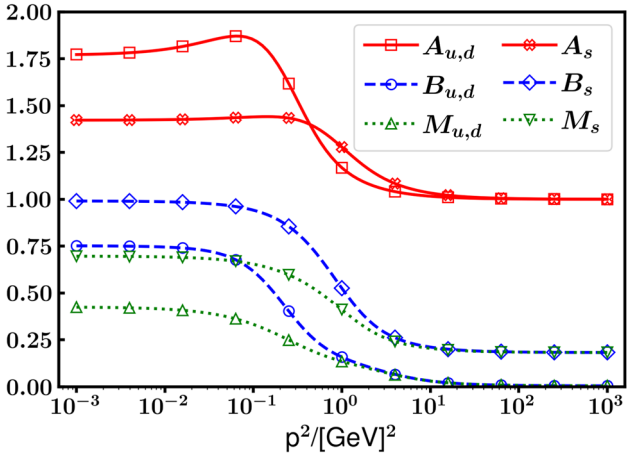

Fig. 2 The dressing functions A (red, square), B (blue, circle) and M (green, upward triangle) of u, d quarks and A (red, cross), B (blue, diamond) and M (green, downward triangle) s quark

As for diquarks, the scalar (0^+) and axial vector (1^+) diquarks' propagators are parameterized as

$$D_{0^+}(k) = \frac{1}{M_{0^+}^2}\mathcal{F}(k^2/\omega_{0^+}^2),$$
$$D_{1^+}^{\mu\nu}(k) = \left(g^{\mu\nu} + \frac{k^\mu k^\nu}{M_{1^+}^2}\right)\frac{1}{M_{1^+}^2}\mathcal{F}(k^2/\omega_{1^+}^2), \tag{3.5}$$

where M_{0^+}, M_{1^+} and ω_{0^+}, ω_{1^+} are the masses and widths of scalar and axial vector diquarks respectively. Since the diquarks originally emanate from T-matrices, their non-trivial on-shell behaviour is completely carried by their Bethe–Salpeter wave functions and their propagators need to satisfy the condition

$$\frac{d}{dk^2}\left(D_{J^P}(k^2)\right)^{-1}|_{k^2=0} = 1 \quad \Rightarrow \quad \omega_{J^P}^2 = \frac{1}{2}m_{J^P}^2 \tag{3.6}$$

for a free particle, see e.g. the appendix of Ref. [43].

The diquark amplitudes are parameterized as

$$\Gamma_{0^+}^a(l, p_d) = ig_{0^+}\gamma_5 C\mathcal{F}(l^2)\lambda^a,$$
$$\Gamma_{1^+}^{a,\mu}(l, p_d) = ig_{1^+}\gamma^\mu C\mathcal{F}(l^2)\lambda^a, \tag{3.7}$$

where l, p_d are the relative momentum between two quarks in diquark and total momentum of diquark respectively. C is the charge conjugation operator. λ^a is the diquark flavor wave function, which is shown explicitly in the appendix, Sec. A.2. $g_{0^+,1^+}$ are the normalization constants of scalar and axial vector diquarks respectively. The diquark normalization condition is given by (Tr means trace over Dirac space)

$$N^2 = \frac{1}{2}\frac{K^\mu}{2K^2}\frac{\partial}{\partial K^\mu}\frac{N_C^{dq}}{N_J}\mathrm{Tr} \int \frac{d^4l}{(2\pi)^4}\Big[\bar{\Gamma}(l,-K_i)S(l+\eta_+K)\Gamma(l,K_i)S^T (-l+\eta_-K)\Big]_{K=K_i}, \tag{3.8}$$

where $N_C^{dq} = 1$ is the normalized color factor of the diquark and $N_J = 2J+1$ counts its degrees of freedom. For the momentum partition parameters of quarks in the diquark we choose $\eta_+ + \eta_- = 1$ and K_i is the on-shell total momentum of diquark $K_i^2 = -M_{J^P}^2$. With the parameters in Table 2, we have explicitly calculated the normalization constants of each diquark and listed the results in Table 2. These constants also determine the coupling strength of each diquark to the two quark lines in the kernel of the quark-diquark Faddeev equation (see above).

The only remaining parameters that are up to now undetermined are the masses of the (flavour anti-symmetric) scalar diquarks $[ud]$, $[ds]$, $[su]$ and the (flavour-symmetric) axial vector diquarks $\{uu\}$, $\{ud\}$, $\{dd\}$, $\{ds\}$, $\{su\}$, $\{ss\}$. Since we work in the isospin symmetric limit these amount to five different mass parameters. These have to be fixed using experimental data for baryon masses. This is discussed in the next section.

4 Mass Spectrum

Using the parameters introduced in the Sec. 3, we solved the Faddeev equation of $N(940)$, $\Delta(1232)$, $\Lambda(1116)$, $\Sigma(1193)$, $\Sigma(1382)$, $\Xi(1315)$, $\Omega(1672)$ and obtained their mass spectrum. To this end, we have adapted the five different diquark masses listed in Table 2 to have a best possible fit for the masses of the five states $N(940)$, $\Delta(1232)$, $\Lambda(1116)$, $\Sigma(1193)$, $\Omega(1672)$. We then vary the best-fit diquark masses by 5% in order to obtain an (obviously naive but still useful) measure for the systematic error of the model. The results

Table 2 Masses (in GeV) and dimensionless coupling constants of diquarks. Whereas the latter are determined entirely by the normalisation condition, Eq. (3.8), the former are fixed by matching the masses of selected baryon octet and decuplet states to experimental data. See main text for details

$M_{[ud]}$	$M_{\{uu\},\{ud\},\{dd\}}$	$M_{[ds],[su]}$	$M_{\{ds\},\{su\}}$	$M_{\{ss\}}$
0.667	0.868	0.950	1.066	1.254
$g_{[ud]}$	$g_{\{uu\},\{ud\},\{dd\}}$	$g_{[ds],[su]}$	$g_{\{ds\},\{su\}}$	$g_{\{ss\}}$
21.52	15.03	17.64	15.97	15.62

Table 3 Masses (in GeV) of selected baryon octet and decuplet states calculated from our quark-diquark Faddeev equation. The errors bars represent a measure for the model uncertainty generated from the variation of our input parameters, the diquark masses, by 5%

	$N(940)$	$\Delta(1232)$	$\Lambda(1116)$	$\Sigma(1193)$	$\Sigma(1385)$	$\Xi(1315)$	$\Omega(1672)$
mass	0.939(74)	1.210(76)	1.116(90)	1.193(90)	1.377(87)	1.301(107)	1.672(111)

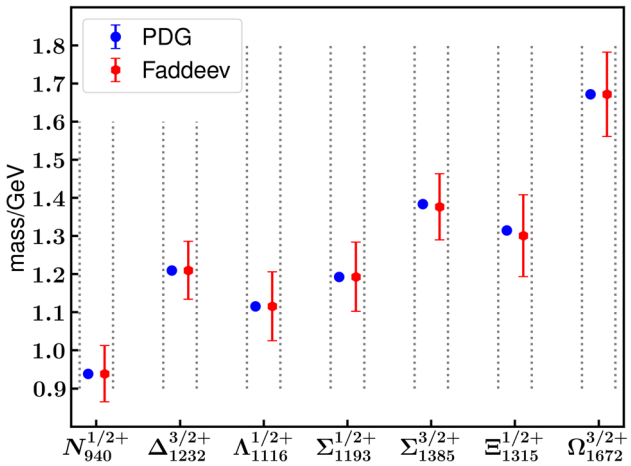

Fig. 3 The mass spectrum of selected baryons calculated from our quark-diquark Faddeev equation (red hexagon) and their comparison with the experimental values (blue circle). Error bars in our results reflect changes induced by variations of the diquark mass parameters by 5%

are listed in Table 3 and are compared to the experimental values in Fig. 3.

From Fig. 3, we find the predicted masses of $\Sigma(1385)$ and $\Xi(1315)$ from our quark-diquark Faddeev equation approach in good agreement with their experimental values. As can be expected, we also find that the baryon masses are quite sensitive to the diquark masses. The 5% variations in the diquark masses lead to variations in the baryon masses in the range of 6–8 %. Fortunately, as we will see in the next sections, the electromagnetic form factors of Λ and Σ will be much less sensitive to these variations.

Finally, we would like to point out a particular appealing property of the diquark-quark model that has been noted already in Ref. [27]: diquark correlations induce the mass split between Λ and Σ already on the level of model approaches such as the one pursued here and also on the level of rainbow-ladder type truncations [5]. In genuine three-body treatments of the Faddeev equation, however, genuine rainbow-ladder type interactions are flavour-blind and one has to go beyond rainbow-ladder to see any splitting [16,59].

We therefore believe that the diquark-quark picture is an excellent starting point to go further and calculate the elastic EMFFs of $\Lambda(1116)$, $\Sigma^+(1189)$, $\Sigma^0(1193)$, $\Sigma^-(1197)$ and the electromagnetic transition form factors $\gamma^{(*)}\Sigma^0(1193) \to \Lambda(1116)$. The good agreement of the mass of the (decuplet) $\Sigma(1385)$ with experiment suggests to go even further and also determine the electromagnetic transition form factors of $\gamma^{(*)}\Sigma(1385) \to \Lambda(1116)$. This is technically much more involved than the octet-octet transition and therefore left for future work. As mentioned in the introduction, in this work we furthermore restrict ourselves to the analysis of the space-like momentum region. Ultimately, out goal is to extend this study to the technically more involved time-like region in future work with applications on the analysis of data from HADES FAIR-phase-0 experiments in mind.

5 Electromagnetic form factors of Λ and Σ

In this section, we will discuss our results for the (space-like) EMFFs of $\Lambda-$ and $\Sigma-$type baryons. This includes the elastic electromagnetic form factors of $\Lambda(1116)$, $\Sigma^+(1189)$, $\Sigma^0(1193)$, $\Sigma^-(1197)$ and the corresponding transition form factors of the only allowed octet transition $\gamma^{(*)}\Sigma^0(1193) \to \Lambda(1116)$.

The electromagnetic currents between two spin-1/2 baryons with initial momentum P_i and mass M_i as well as final momentum P_f and mass M_f can be written as (e is the electric charge of positron)

$$\langle P_f | J^\mu | P_i \rangle = ie\bar{u}(P_f) \left(\gamma_T^\mu F_1(Q^2) \right.$$

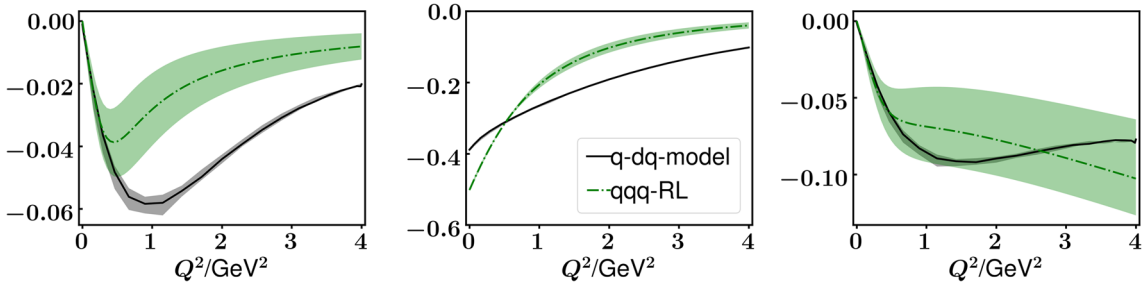

Fig. 4 The elastic electromagnetic form factors G_E (left) and G_M (center) and their ratio G_E/G_M (right) for the $\Lambda(1116)$. The magnetic form factor is expressed in units of the nuclear magneton. The black lines are our results from the quark-diquark Faddeev equation ('q-dq-model'). The black band represents the error band arising from a variation of diquark mass parameters by 5%. The green dash-dotted lines and the corresponding error band are results from a three-body Faddeev equation calculation ('qqq-RL') using an underlying effective running coupling in rainbow-ladder (RL) approximation [15]

$$+\frac{1}{M_f+M_i}\sigma^{\mu\nu}Q_\nu F_2(Q^2)\Big)\,u(P_i), \quad (5.1)$$

where $Q = P_f - P_i$ is the photon momentum and $\gamma_T^\mu = \left(g^{\mu\nu} - Q^\mu Q^\nu/Q^2\right)\gamma_\nu$. The Dirac, Pauli form factors F_1, F_2 and the Sachs electric, magnetic form factors G_E, G_M are related via

$$G_E = F_1 - \frac{Q^2}{(M_f+M_i)^2}F_2\,, \quad (5.2)$$

$$G_M = F_1 + F_2\,. \quad (5.3)$$

Here we should comment on the unit of the magnetic form factor. From the electromagnetic current, Eq.(5.1), one reads of that the Pauli form factor F_2 is expressed in units of $e\hbar/(M_f+M_i)$ where $\hbar$ is the Plank constant. However, conventionally, one prefers to use common units for the magnetic form factors of all baryons and expresses the magnetic moment in units of the nuclear magneton $e\hbar/2M_N$ where M_N is the proton mass. In this work, we follow this convention and also express the magnetic form factors of Λ, Σ and $\gamma^{(*)}\Sigma^0(1193) \to \Lambda(1116)$ in units of the nuclear magneton. Thus the magnetic form factors G_M of Eq. (5.3) are further multiplied by a factor $2M_N/(M_f+M_i)$.

Technically, the procedure to couple an external field to a Bethe–Salpeter equation is called *gauging* of the equation and was introduced in Refs. [60–64]. This procedure ensures gauge invariance, prevents over-counting of diagrams and leads to charge conservation. The diagrammatic elements we need to calculate the EMFFs in this approach have been discussed in detail in many works, see e.g. [5,53,63] and are summarised in Appendix B for the convenience of the reader. These expressions also contain a number of further parameters that are fitted to the nucleon's electromagnetic form factors. This is discussed in Appendix B, where we also display the corresponding results.

5.1 Elastic EMFFs of Λ and Σ

Although we cannot observe the elastic EMFFs of Λ and Σ experimentally, they are still worth investigating for two reasons. On the one hand, they express our knowledge of the electromagnetic properties of the Λ and Σ. Systematic comparison with other electromagnetic form factors within the baryon multiplets might reveal important information of the flavour dependence of their internal dynamics. On the other hand, the elastic EMFFs are a convenient tool to normalize the Faddeev amplitudes of Λ and Σ^0, which is in turn a prerequisite for the calculation of their transition form factors $\gamma^{(*)}\Sigma(1193) \to \Lambda(1116)$.

Since the Λ and Σ^0 are charge zero, we normalize their Faddeev amplitudes from the flavor separated electric form factors [48]:

$$G_E(Q^2) = e_u G_E^u(Q^2) + e_d G_E^d(Q^2) + e_s G_E^s(Q^2), \quad (5.4)$$

where e_u, e_d, e_s are the electric charges in units of e and $G_E^u(Q^2)$, $G_E^d(Q^2)$, $G_E^s(Q^2)$ are the electric charge form factors of u, d, s quarks respectively. The normalization condition of Λ and Σ^0 is then given by:

$$G_E^u(0) = G_E^d(0) = G_E^s(0) = 1. \quad (5.5)$$

A convenient cross-check is provided by the fact that the normalization constant of Σ^0 calculated from Eq. (5.5) has to be the same as the normalization constants of Σ^+ and Σ^- calculated from the usual normalization conditions $G_E(0) = 1$ for Σ^+ and $G_E(0) = -1$ for Σ^-. This is indeed the case in our calculation. The results for the elastic EMFFs of the Λ and Σ triplet are shown in Figs. 4 and 5 respectively. As with the baryon masses, our error bands arise from varying the diquark mass parameters by 5%.

In Fig. 4, we compare the EMFFs of the $\Lambda(1116)$ from our quark-diquark Faddeev equation with corresponding results from a three-body Faddeev equation [15]. For the electric form factor, we find almost identical results for small momen-

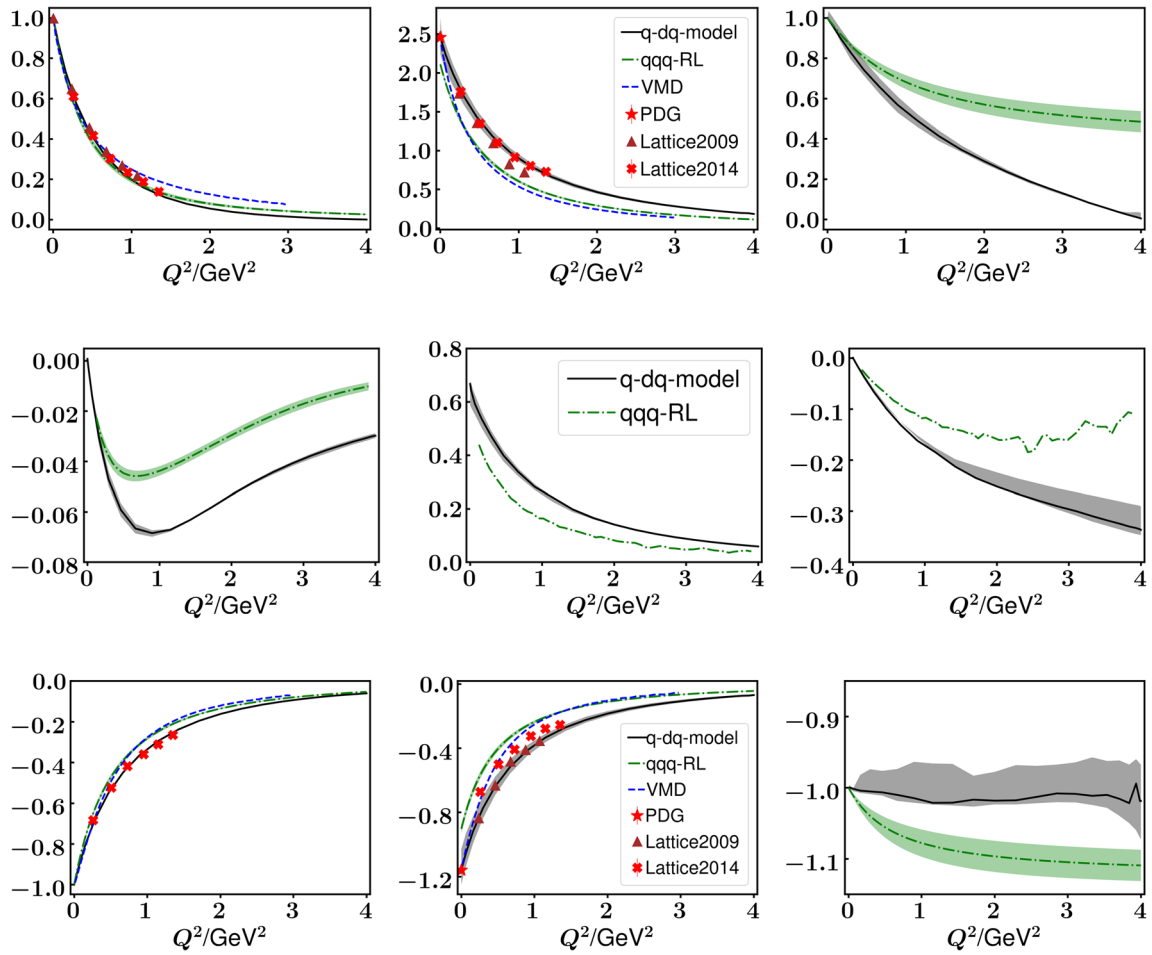

Fig. 5 The elastic electromagnetic form factors G_E (left), G_M (center) and their ratio (right) of $\Sigma^+(1189)$ (top), $\Sigma^0(1193)$ (middle) and $\Sigma^-(1197)$ (bottom). The magnetic form factor is expressed in units of the nuclear magneton. The black lines are our results from the quark-diquark Faddeev equation ('q-dq-model'). The black bands representan error estimate arising from the variation of diquark masses by 5%. The red star is the magnetic moment of $\Lambda^0(1116)$ from PDG [65]. Red crosses [13,14] and brown triangles [66] represent results from Lattice QCD calculations. The green dash-dotted lines and bands ('qqq-RL') are again results from the three-body Faddeev equation [15]. The blue dashed lines are results computed from a vector-meson dominance model [19]

tum transfer Q^2. This also implies that the two methods predict the same electric charge radius of the $\Lambda(1116)$. The large momentum behaviour, however, is similar in its functional form but markedly different in size. A similar difference can be observed for the magnetic form factor. This difference in fall-off may be related to the different internal dynamics of the two approaches (i.e. the quark-gluon interaction explicit in the three-body approach and implicit in the quark-diquark model) but also may be generic to the differences between a three-body and a quark-diquark picture (or a combination of both). In our results for the corresponding nucleon EMFFs, discussed in Appendix Sect. B.6, we do not see such large differences. Thus a definitive answer to this question may have to wait until a quark-diquark calculation using the same effective model as the three-body Faddeev equation is available.[1]

At small momenta the magnetic form factor G_M of our quark-diquark Faddeev equation predicts a smaller decrease rate than the three-body Faddeev equation method. This might be an effect due to diquark correlations decreasing the size of the Λ as compared to the three-quark picture. As a result, the magnetic form factor predicted by our quark-diquark Faddeev equation is harder than the three-body Faddeev equation

[1] Note also that the present approach is not suitable (and not intended) to study the behaviour of the form factors in the very large, perturbative momentum region, since our ansaetze for the quark dressing functions do not include the proper logarithmic perturbative running. This is different for more advanced diquark-quark approaches and the three-body Faddeev approach using an underlying effective running coupling, see e.g. [5] for a detailed discussion on the different approaches.

Table 4 In the upper two tables we display our results for the mean-squared magnetic and electric charge radii expressed in units of fm^2. We compare our results with the ones of the three-body approach [15], available VMD results [11,20], from chiral perturbation theory (ChPT) [17] and dispersion theory (disp) [24] and the only available experimental result for the Σ^- [65]. In the lower table we display our results for the magnetic moments in units of the nuclear magneton and compare again with the three-body approach [15] and experimental results [65]

	$\langle r_E^2\rangle$	$\langle r_E^2\rangle_{3b}$	$\langle r_E^2\rangle_{VMD}$	$\langle r_E^2\rangle_{ChPT}$	$\langle r_E^2\rangle_{disp}$	$\langle r_E^2\rangle_{PDG}$
Λ	0.036(14)	0.04(1)	0.012	0.11(2)	–	–
Σ^+	0.469(9)	0.56(3)	0.80(2)	0.60(2)	–	–
Σ^0	0.068(9)	0.057(8)	0.10(1)	−0.03(1)	–	–
Σ^-	0.353(26)	0.45(3)	0.70(2)	0.67(3)	–	0.61(15)

	$\langle r_M^2\rangle$	$\langle r_M^2\rangle_{3b}$	$\langle r_M^2\rangle_{VMD}$	$\langle r_M^2\rangle_{ChPT}$	$\langle r_M^2\rangle_{disp}$
Λ	0.120(76)	0.21(1)	0.18	0.48(9)	0.464(2)
Σ^+	0.374(41)	0.43(2)	–	0.80(5)	–
Σ^0	0.201(169)	0.39(3)	–	0.45(8)	–
Σ^-	0.459(122)	0.50(1)	–	1.20(13)	–

	μ	μ_{3b}	μ_{PDG}
Λ	−0.390(3)	−0.435(5)	−0.613(4)
Σ^+	2.422(180)	1.82(2)	2.458(10)
Σ^0	0.630(48)	0.521(1)	–
Σ^-	−1.145(106)	−0.78(2)	−1.160(25)

prediction. Similar effects are seen in the nucleon, cf. our discussion in Appendix B.6.

In Fig. 5, we compare the EMFFs of Σ^+, Σ^0 and Σ^- from our quark-diquark Faddeev method with that from other theoretical methods such as the three-body Faddeev approach [15], Lattice QCD [13,14,66] and a vector-meson dominance model [19]. We also display the experimental values of the magnetic moment at zero momentum [65]. We obtain good agreement with the lattice calculations of G_E, G_M for Σ^+ and Σ^-. We interpret this as further indication that the diquark-quark picture is valid and our model provides for reasonable results.

An interesting difference can be seen in the ratios $\mu * G_E/G_M$ for the $\Sigma^{+,0}$ and Σ^- baryons. The ratio for Σ^+ decreases monotonically from one to zero in our quark-diquark Faddeev framework, i.e. the electric charge form factor G_E decreases much faster than the magnetic form factor G_M. The three-body Faddeev equation framework [15] also exhibits a similar phenomenon, albeit with a less rapid decrease in the ratio. In contrast, the ratio for Σ^- starts at minus one and stays constant within error bars in our quark-diquark Faddeev framework, i.e. the electric and magnetic form factors decreases with the same rate. In the three-body Faddeev framework, the electric form factors even decrease slower than the magnetic form factors. Consequently, both the quark-diquark and three-body Faddeev frameworks display a larger decrease rate of electric form factors G_E in Σ^+. while they both show equal or smaller decrease rate of G_E in Σ^- comparing to the corresponding magnetic form factors G_M. A similar observation has been made in Ref. [19] in the time-like momentum region. A possible explanation for this behaviour starts from the observation that the Σ^+ and Σ^- have flavor wave functions of the same structure, see Eq. (2.6), but with the two u quarks in Σ^+ replaced by two d quarks in Σ^-. The three possible flavour structures are dominated by the scalar $[su]$ diquark in the Σ^+ baryon and the scalar $[ds]$ in Σ^- [35]. Thus, approximately, the Σ^+ can be viewed as a two-body state composed of a u quark (with charge $+\frac{2e}{3}$) and a heavier $[su]$ diquark (with charge $+\frac{e}{3}$). The Σ^- is well represented by a d quark (with charge $-\frac{e}{3}$) and a heavier $[ds]$ diquark (with charge $-\frac{2e}{3}$). Therefore, viewed from the rest frame of the respective diquarks, twice the amount of charge is located in the center of the Σ^- than in the center of the Σ^+ and the corresponding electric charge form factor G_E of Σ^+ will decrease more rapidly than that of the Σ^-, while the magnetic form factor G_M of Σ^+ will decrease slower than that of Σ^-. In combination, this leads to the different behaviors of the ratio of EMFFs. The Σ^0 is in-between and therefore its form factor ratio falls off less rapidly than the one of the Σ^+. Similar qualitative features have been observed in lattice calculations [13,14,67].

This qualitative discussion can be made more quantitative by determining the corresponding electric and magnetic charge radii. The mean-squared charge radii can be extracted from the form factors $G = G_{E,B}$ via

$$\left\langle r^2 \right\rangle = -6 \frac{d}{dQ^2} \frac{G(Q^2)}{G(0)} \bigg|_{Q^2=0}. \tag{5.6}$$

where the term $G(0)$ is set to one for form factors constraint to vanish at the origin. The obtained mean-squared charge radii of Λ and Σ from the quark-diquark equations are listed in Table 4 together with our results for the magnetic moments and their comparison with the corresponding results in the three body Faddeev approach [15], available VMD results [11,20], from chiral perturbation theory (ChPT) [17] and dispersion theory (disp) [24]and experimental values from PDG [65]. Qualitatively, our results for the electric and magnetic charge radii agree very well with the ones from the three-body approach and the VMD-results, whereas the values from ChPT for most hyperons and the one from dispersion theory for the Λ are larger. Taken at face value this points towards possible meson cloud effects that are not accounted for in our approach and therefore result in somewhat too small charge radii.

It is nevertheless interesting to note that in both DSE/BSE approaches (and the VMD calculation) the electric and magnetic charge radii of the Λ and the Σ^0 are quite different, although the quark content of both types of baryons is the same. As already discussed in Ref. [67], quark model explanations of this difference usually fall short (see also [15] for a discussion). Also different intermediate virtual transitions between baryons (discussed in [67]) cannot be the prime source of the difference in radii since both, the three-body Faddeev approach and our quark-diquark picture reproduce such a difference without baryonic intermediate states. Instead, our results give further support to the conclusion of Ref. [15] that the difference may be solely generated by the different symmetries in the flavour structure of the states. This needs to be explored further.

An interesting difference between the three-body approach and our quark-diquark model concerns the magnetic moments. Here, the three-body results fall drastically short in comparison with the experimental results, whereas we could reproduce those. The general explanation of the failure of the three-body approach is missing pion and kaon cloud effects. A pure quark-core calculation has to fall short of the experimental magnetic moments, as convincingly argued in many works, see e.g., [15,40,68] and references therein. So why is this different in the quark-diquark model? It seems as if part of the effects of the pion and meson cloud, in particular static effects, can be accommodated by the many parameters inherent of the model. Thus magnetic moments can be 'made' right by a suitable choice of parameters. Nevertheless, the explicit momentum dependent dynamics of the related diagrams in form factor calculations is not included in our model. Consequently, the smaller values of both approaches for the electric charge radius of the Σ^- as compared to experiment (and ChPT) may be interpreted as due to missing meson cloud effects, as already discussed above.

In order to make our numerical results for the electromagnetic form factors of Λ and Σ available for comparisons and also for further calculations, we provide corresponding fits. To this end we use similar fit functions as in Ref. [15]:

$$G(Q^2) = \frac{n_0 + n_1 Q^2}{1 + d_1 Q^2 + d_2 Q^4 + d_3 Q^6}. \tag{5.7}$$

The best-fitted parameters for Λ and Σ are given in Table 5 in Appendix C.

5.2 Transition form factors of the process $\gamma^{(*)}\Sigma^0 \to \Lambda$

With the normalized Faddeev amplitudes of Σ^0 and Λ at hand, we can go further and calculate the electromagnetic transition form factors of $\gamma^{(*)}\Sigma^0 \to \Lambda$ in the space-like momentum region. Our results are shown in Fig. 6 and compared with corresponding results from the three-body Faddeev equation approach [16]. At non-vanishing momenta, these form factors have also been studied in [18] with particular emphasis on disentangling contributions from the quark core with meson cloud contributions, and in Ref. [22] using dispersive methods. In Fig. 6 we also included latest results from the dispersive analysis of Ref. [25] with the value of G_M at zero momentum fixed in Ref. [22].

In principle, the electric transition form factor G_E of $\gamma^{(*)}\Sigma^0 \to \Lambda$ should be exactly equal to zero at the on-shell point of the photon $Q^2 = 0$, as can be seen from the dispersive results [25]. In practice, numerical errors are large at this point and consequently this is neither exactly the case in our calculation, nor in the three-body Faddeev results. Our numerical error is somewhat larger than in the three-body case but still tolerable. Overall, we obtained results for G_E with the same qualitative behaviour as the one from the three-body Faddeev equation: the general magnitude of G_E is small and decrease slowly in the medium momentum region. Differences in magnitude in the medium and large momentum region are again visible similar as for the elastic form factors. Overall we find from both approaches that the electric transition of $\gamma^{(*)}\Sigma^0 \to \Lambda$ falls of slowly and therefore the transition is quite localized.

Note that we also further confirm an important difference to quark model calculations already discussed in [16]: whereas in typical quark model setups the baryons are entirely composed of s- and d-waves, sizeable contributions from p-waves appear naturally in both, the relativistic three-body and the relativistic quark-diquark Bethe–Salpeter approach. These are responsible for our non-zero result of the electric transition form factor. In non-relativistic quark-models, similar results can only be obtained invoking unnaturally strong d-wave contributions or including meson cloud effects [18].

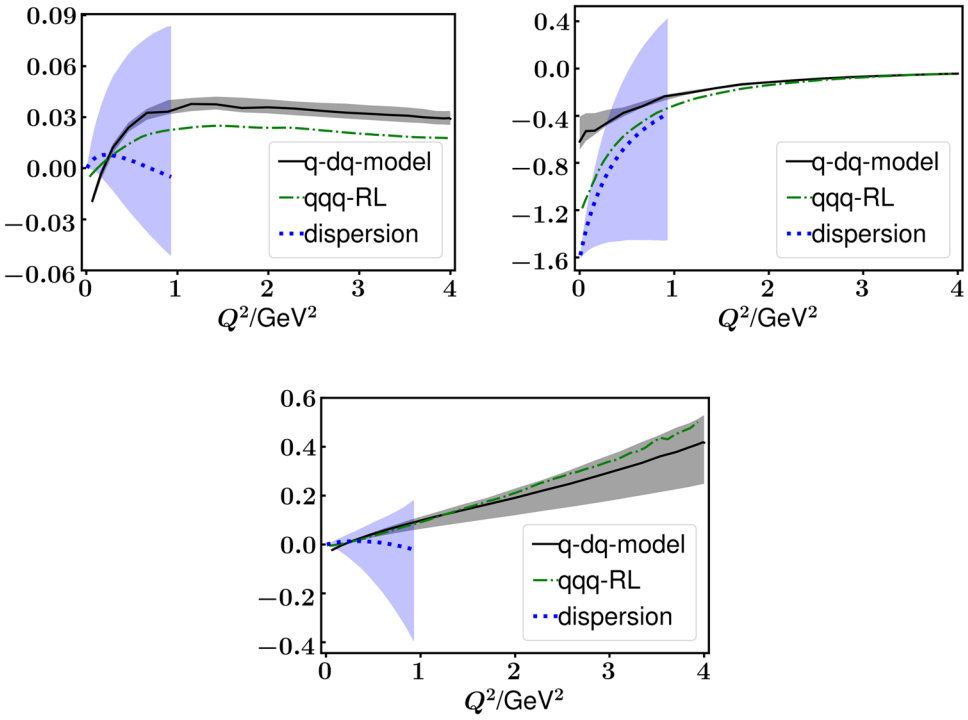

Fig. 6 The electromagnetic transition form factors G_E (upper panel, left) and G_M (upper panel, right) and their ratio (lower panel) of the process $\Sigma^0 \to \Lambda$. The magnetic form factor is again expressed in units of the nuclear magneton. The black lines are our results from the quark-diquark Faddeev equation ('q-dq-model'). The black bands represent an error-estimate based on the variation of diquark mass parameters by 5%. The green dash-dot lines are the results from the three-body Faddeev equation ('qqq-RL') again using an effective running coupling in rainbow-ladder ('RL') approximation discussed in Ref. [16]. The dispersive result (blue dotted line with blue error band) is taken from Ref. [25]

As for the magnetic transition form factor G_M of $\gamma^{(*)}\Sigma^0 \to \Lambda$, the result calculated from the quark-diquark Faddeev equation is about a factor of two smaller at vanishing momentum than the one calculated from the three-body Faddeev equation. The dispersive value, estimated in Ref. [22] from the experimental width of the decay $\Sigma^0 \to \Lambda\gamma$, is of the same order of magnitude than the three-body result.[2] At finite momenta, the error of the dispersive result increases rapidly. Thus, given the current level or precision, dispersion theory cannot reasonably discriminate between our quark-diquark model result and the three-body result. At medium and large momenta $Q^2 \geq 2$ GeV^2, the G_M calculated from quark-diquark Faddeev equation and the three-body Faddeev equation meet each other. In the third diagram of Fig. 6 we also show the form factor ratio, which rises monotonically as momentum increases. In this plot we did not include the error estimate of the dispersive result, but it is clear from the upper panel that the dispersive result can only be trusted for very small momenta.

6 Summary

In this work, we extended the quark-diquark Faddeev approach to the strange baryon sector and determined the elastic electromagnetic form factors of $\Lambda(1116)$, $\Sigma^+(1189)$, $\Sigma^0(1193)$ and $\Sigma^-(1197)$. Our results agree well on a quantitative level with lattice QCD calculations, where available. Interesting differences appear when comparing our results with that calculated from a three-body Faddeev approach. We find the same overall running, albeit with sizeable differences in magnitude in certain momentum ranges that are different for different baryons. In general, the quark-diquark Faddeev method predicts harder form factors than that from three-body Faddeev approach calculations.

A very interesting observation is the different running with photon momentum of the ratio of EMFFs for $\Sigma^{+,0}$ and Σ^-: for Σ^+ and Σ^0 it decreases monotonically while for Σ^- it remains constant. This can be explained by the different diquark correlations inside these hyperons.

Furthermore, we computed the electromagnetic transition form factors for $\gamma^{(*)}\Sigma^0 \to \Lambda$. The obtained results from quark-diquark Faddeev model have the same behavior as those calculated from the three-body Faddeev approach, however again we observe sizeable difference in magnitude. Overall, we find a localized electric transition form factor in both approaches.

In the future, we plan to extend our calculations from the space-like to the time-like photon momentum. To this end we also plan to include effects due to the appearance of vector meson resonances in the transverse part of the quark-photon vertex that are currently not taken into account. It is furthermore useful to compare to other electromagnetic transition form factors such as $\Delta \to N$ and $\Sigma(1385) \to \Lambda$ to obtain

[2] Note that Refs. [22,25] use a different normalisation than we do, thus their $\kappa \approx 1.98$ corresponds to our $\kappa \frac{2m_p}{m_\Lambda + m_\Sigma} \approx 1.61$.

more insight into the role played by the strange quark inside baryons.

Acknowledgements We are grateful for helpful discussions with G. Eichmann, P. Cheng and Z. Yao. This work is supported by a Sino-German (CSC-DAAD) Postdoc Scholarship and project funding from the Helmholtz Forschungsakademie Hessen für FAIR (HFHF).

Funding Open Access funding enabled and organized by Projekt DEAL.

Data Availability Statement This manuscript has no associated data or the data will not be deposited. [Authors' comment: Data are available from the authors upon request.]

A Computing ingredients for quark-diquark Faddeev equation

A.1 The basis for quark-diquark Faddeev amplitudes of Λ and Σ

Denoting

$$p_\perp^\mu = p^\mu - \hat{P}^\mu \left(p \cdot \hat{P}\right), \ \gamma_\perp^\mu = \gamma^\mu - \hat{P}^\mu \left(\gamma \cdot \hat{P}\right), \\ \hat{P}^\mu = \frac{P^\mu}{iM}, \tag{A.1}$$

then for the baryon with total spin $J = \frac{1}{2}$ and positive parity, the matrix valued functions for scalar and axial-vector diquarks can be expanded as:

$$\Phi_{0^+}(p, P) = \sum_{i=1}^{2} f_{0^+}^i(p, P)\mathcal{S}_i(p, P), \tag{A.2a}$$

$$\Phi_{1^+}^\mu(p, P) = \sum_{i=1}^{6} f_{1^+}^i(p, P)\mathcal{A}_i^\mu(p, P), \tag{A.2b}$$

with dressing functions $f_{0^+,1^+}^i$ and Dirac tensors

$$\mathcal{S}_1(p, P) = \Lambda^+, \tag{A.3a}$$

$$\mathcal{S}_2(p, P) = i\gamma \cdot p^\perp \Lambda^+, \tag{A.3b}$$

$$\mathcal{A}_{1\mu}(p, P) = -\gamma_5 \gamma_\mu^\perp \Lambda^+, \tag{A.4a}$$

$$\mathcal{A}_{2\mu}(p, P) = i P_\mu \gamma_5 \Lambda^+, \tag{A.4b}$$

$$\mathcal{A}_{3\mu}(p, P) = i p_\mu^\perp \gamma_5 \Lambda^+, \tag{A.4c}$$

$$\mathcal{A}_{4\mu}(p, P) = -i\gamma_5 \gamma_\mu^\perp \gamma \cdot p^\perp \Lambda^+, \tag{A.4d}$$

$$\mathcal{A}_{5\mu}(p, P) = -P_\mu \gamma_5 \gamma \cdot p^\perp \Lambda^+, \tag{A.4e}$$

$$\mathcal{A}_{6\mu}(p, P) = -p_\mu^\perp \gamma_5 \gamma \cdot p^\perp \Lambda^+. \tag{A.4f}$$

A.2 Diquark flavor wave function

We denoted the flavor wave functions of diquarks as λ^a:

$$\lambda^{[ud]} = \frac{1}{\sqrt{2}} \begin{bmatrix} 0 & 1 & 0 \\ -1 & 0 & 0 \\ 0 & 0 & 0 \end{bmatrix}, \lambda^{[ds]} = \frac{1}{\sqrt{2}} \begin{bmatrix} 0 & 0 & 0 \\ 0 & 0 & 1 \\ 0 & -1 & 0 \end{bmatrix}, \\ \lambda^{[su]} = \frac{1}{\sqrt{2}} \begin{bmatrix} 0 & 0 & -1 \\ 0 & 0 & 0 \\ 1 & 0 & 0 \end{bmatrix}, \tag{A.5}$$

$$\lambda^{\{uu\}} = \begin{bmatrix} 1 & 0 & 0 \\ 0 & 0 & 0 \\ 0 & 0 & 0 \end{bmatrix}, \lambda^{\{ud\}} = \frac{1}{\sqrt{2}} \begin{bmatrix} 0 & 1 & 0 \\ 1 & 0 & 0 \\ 0 & 0 & 0 \end{bmatrix}, \\ \lambda^{\{dd\}} = \begin{bmatrix} 0 & 0 & 0 \\ 0 & 1 & 0 \\ 0 & 0 & 0 \end{bmatrix}, \tag{A.6}$$

$$\lambda^{\{su\}} = \frac{1}{\sqrt{2}} \begin{bmatrix} 0 & 0 & 1 \\ 0 & 0 & 0 \\ 1 & 0 & 0 \end{bmatrix}, \lambda^{\{ds\}} = \frac{1}{\sqrt{2}} \begin{bmatrix} 0 & 0 & 0 \\ 0 & 0 & 1 \\ 0 & 1 & 0 \end{bmatrix}, \\ \lambda^{\{ss\}} = \begin{bmatrix} 0 & 0 & 0 \\ 0 & 0 & 0 \\ 0 & 0 & 1 \end{bmatrix}, \tag{A.7}$$

B Computing the electromagnetic form factors in quark-diquark Faddeev equation approach

The electromagnetic current in the quark-diquark Faddeev equation has five types of diagrammatic contributions arising from the gauging technique [60–64,69]. The photon can interact: (1), with a bystander quark; (2), with a diquark (including the photon induced transition between different diquarks); (3) with the exchanged quark; (4) with diquark the amplitude and (5) with the conjugated diquark amplitude. These are depicted in Fig. 7. Writing down the expressions explicitly, they are given by

$$J_{\alpha\beta}^\mu(Q^2) = \int_{p_f} \int_{p_i} \Big[\bar{\Phi}^a(p_f, P_f) X^{\mu,ab}(p_f, p_i, P_f, P_i) \\ \Phi^b(p_i, P_i)\Big]_{\alpha\beta}. \tag{B.1}$$

Here p_i, p_f are the relative momentum of initial and final states and P_i, P_f are the total momentum of initial and final states, $P_f = P_i + Q$. $\alpha, \beta = 1, \ldots, 4$ are the

quark indices and a, b are the diquark indices. The quantity $X^{\mu,ab}(p_f, p_i, P_f, P_i)$ is given by

$$X^{\mu,ab} = X_q^{\mu,ab}\,(2\pi)^4\delta^4(p_f - p_i - (1-\eta)Q) + X_{dq}^{\mu,ab}\,(2\pi)^4\delta^4(p_f - p_i + \eta Q) + X_K^{\mu,ab}\,. \tag{B.2}$$

$$X_{q,\alpha\beta}^{\mu,ab} = \Big[S(p_+)\Gamma_q^{\mu}(p_+, p_-)S(p_-)\Big]_{\alpha\beta} D^{ab}(p_{d-})\,, \tag{B.3}$$

$$X_{dq,\alpha\beta}^{\mu,ab} = [S(p_-)]_{\alpha\beta}\Big[D^{aa'}(p_{d+})\Gamma_{dq}^{\mu,a'b'}D^{b'b}(p_{d-})\Big]\,, \tag{B.4}$$

$$X_{K,\alpha\beta}^{\mu,ab} = D^{aa'}(p_{d+})\Big[S(p_+)K^{\mu,a'b'}S(p_-)\Big]_{\alpha\beta} D^{b'b}(p_{d-})\,, \tag{B.5}$$

where

$$p_- = p_i + \eta P_i\,, \qquad p_{d-} = -p_i + (1-\eta)P_i\,,$$
$$p_+ = p_f + \eta P_f\,, \qquad p_{d+} = -p_f + (1-\eta)P_f\,.$$

As for the gauged kernel,

$$K^{\mu,ab} = K_{EX}^{\mu,ab} + K_{SG}^{\mu,ab} + K_{\overline{SG}}^{\mu,ab}, \tag{B.6}$$

where

$$K_{EX}^{\mu,ab} = \Gamma_{dq}^{b}(p_1, p_{d-})\Big[S(q')\Gamma_q^{\mu}(q', q)S(q)\Big]^T \bar{\Gamma}^a(p_2, p_{d_+})\,, \tag{B.7}$$

$$K_{SG}^{\mu,ab} = M^{\mu,b}(k_1, p_{d-}, Q)S^T(q')\bar{\Gamma}^a(p_2, p_{d+})\,, \tag{B.8}$$

$$K_{\overline{SG}}^{\mu,ab} = \Gamma^b(p_1, p_{d-})S^T(q)\bar{M}^{\mu,a}(k_2, p_{d+}, Q)\,, \tag{B.9}$$

and

$$q = p_{d-} - p_+\,, \qquad p_1 = \frac{p_+ - q}{2}\,, \qquad p_2 = \frac{p_- - q'}{2}\,,$$
$$q' = p_{d+} - p_-\,, \qquad k_1 = \frac{p_+ - q'}{2}\,, \qquad k_2 = \frac{p_- - q}{2}\,.$$

In the following we discuss these diagrams in turn.

B.1 Quark-photon diagram

The quark-photon current contribution is

$$J_1^{\mu}(Q^2) = \int_{p_i}\Big[\bar{\Phi}^a(p_f, P_f)\Big[S(p_+)\Gamma_q^{\mu}(p_+, p_-)S(p_-)\Big] D^{ab}(p_{d-})\Phi^b(p_i, P_i)\Big], \tag{B.10}$$

with $p_f = p_i + (1-\eta)Q$. The quark-photon vertex involved in this diagram has to satisfy the Ward–Takahashi identity:

$$i\,Q_\mu\Gamma^{\mu}(p_2, p_1) = S^{-1}(p_2) - S^{-1}(p_1). \tag{B.11}$$

To this end we employ the Ball–Chiu solution of this identity:

$$\Gamma^{\mu}(p_2, p_1) = \gamma^{\mu}\Sigma_A + (p_1 + p_2)^{\mu}\left[\frac{\not{p}_1 + \not{p}_2}{2}\triangle_A - i\triangle_B\right] + \Gamma_T^{\nu}(p2, p1), \tag{B.12}$$

with

$$\Sigma_F(p_2, p_1) = \frac{F(p_2^2) + F(p_1^2)}{2}, \qquad \triangle_F = \frac{F(p_2^2) - F(p_1^2)}{p_2^2 - p_1^2}. \tag{B.13}$$

The eight amplitudes in the transverse parts $\Gamma_T^{\nu}(p2, p1)$ cannot be constrained by the WTI and we ignore them in this work. Note, however, that due to the appearance of vector meson contributions, these will certainly play an important role in the time-like momentum region and we therefore plan to include those in future work.

B.2 Diquark-photon diagram

The diquark-photon current contribution is

$$J_{\alpha\beta}^{\mu}(Q^2) = \int_{p_i}\Big[\bar{\Phi}^a(p_f, P_f)[S(p_-)]_{\alpha\beta} \Big[D^{aa'}(p_{d+})\Gamma_{dq}^{\mu,a'b'}D^{b'b}(p_{d-})\Big]\Phi^b(p_i, P_i)\Big], \tag{B.14}$$

with $p_f = p_i - \eta Q$. The diquark-photon vertex again satisfies a Ward-Takahashi identity. For the scalar diquark, it is the electromagnetic vertex for spin-0 particle:

$$Q_\mu\Gamma_{sc}^{\mu}(k, Q) = D^{-1}(k_+) - D^{-1}(k_-) = Q_\mu\left[2k^{\mu}\triangle_{D^{-1}}\right], \tag{B.15}$$

with $Q = k_+ - k_-$ and $k = (k_- + k_+)/2$ and $\triangle_{D^{-1}}$ is defined as in Eq. (B.13). This relation is strictly valid for point-like particles. Considering the internal structure of our scalar diquarks, we added the following form factor:

$$\Gamma_{0^+}^{\mu}(k, Q) = 2k^{\mu}\triangle_{D_{0^+}^{-1}}\frac{1}{1 + Q^2/\Lambda_{0^+}^2}, \tag{B.16}$$

The scale $\Lambda_{0^+}^2$ is a free parameter and needs to be determined by comparison with experimental data for the electromagnetic form factors. Here, we choose the electromagnetic form factors of nucleons as benchmarks and obtain $\Lambda_{0^+}^2 = 1.024$ GeV^2.

For axial vector diquark, we adopted the form of electromagnetic vertex for spin-1 particle [70]. The axial vector diquark-photon vertex is (denote $T_{\mu\nu}(Q) = \delta_{\mu\nu} - Q_\mu Q_\nu/Q^2$)

$$\Gamma_{1^+}^{\mu,\alpha\beta}(k, Q) = (p_i + p_f)^{\mu}T^{\alpha\gamma}(p_f)T^{\gamma\beta}(p_i)\triangle_{D_{1^+}^{-1}}F_1(Q^2)$$

$$+\left(T^{\mu\beta}(p_i)T^{\alpha\gamma}Q_\gamma - T_{\mu\alpha}(p_f)T_{\beta\gamma}Q_\gamma\right)\triangle_{D_{1^+}^{-1}}F_2(Q^2)$$
$$-(p_i+p_f)^\mu T^{\alpha\gamma}(p_f)Q_\gamma T^{\beta\lambda}(p_i)Q_\lambda\triangle_{D_{1^+}^{-1}}F_3(Q^2)\,. \tag{B.17}$$

The $F_i(Q^2)$ relate with the multipole form factors of axial vector diquark as

$$F_1(Q^2) = G_e(Q^2) - \frac{2}{3}\tau G_q(Q^2)\,,\ \tau = \frac{Q^2}{4M_{1^+}^2}\,, \tag{B.18}$$
$$F_2(Q^2) = G_m(Q^2)\,, \tag{B.19}$$
$$F_3(Q^2) = \frac{1}{2M_{1^+}^2}\frac{-G_e(Q^2)+G_m(Q^2)+(1+2/3\tau)G_q(Q^2)}{1+\tau}\,. \tag{B.20}$$

We parameterized the multipole form factors of axial vector diquark as

$$G_e(Q^2) = \frac{1}{\left(1+Q^2/\Lambda_{1^+}^2\right)^2}\,, G_m(Q^2) = \frac{g_m}{\left(1+Q^2/\Lambda_{1^+}^2\right)^2}\,,$$
$$G_q(Q^2) = \frac{-g_q}{\left(1+Q^2/\Lambda_{1^+}^2\right)^2}\,. \tag{B.21}$$

Similar as above, we determine the free parameter by best fits to the electromagnetic form factors of nucleons. We obtain $\Lambda_{1^+}^2 = 0.582\ \mathrm{GeV}^2$, $g_m = 1.21$ and $g_q = 0.899$.

The last diquark-photon vertex is the scalar-axial vector diquark transition vertex, which cannot be obtained from gauged technique. This vertex is purely transverse and cannot be constrained by the current conservation:

$$Q_\mu\Gamma_{sa}^{\mu,5\beta} = Q_\mu\Gamma_{as}^{\mu,\alpha 5} = 0. \tag{B.22}$$

In analogy to the $\rho \to \pi\gamma$ decay, the transition vertex is given by the Lorentz structure

$$\Gamma_{sa}^{\mu,5\beta}(p_2,p_1) = i\varepsilon^{\mu\beta\rho\sigma}Q^\rho(p_1+p_2)^\sigma \frac{\kappa_{sa}}{2M_{1^+}}\frac{1}{\left(1+Q^2/\Lambda_{sa}^2\right)^2}, \tag{B.23}$$

$$\Gamma_{as}^{\mu,\alpha 5}(p_2,p_1) = -i\varepsilon^{\mu\beta\rho\sigma}Q^\rho(p_1+p_2)^\sigma \frac{\kappa_{sa}}{2M_{1^+}}\frac{1}{\left(1+Q^2/\Lambda_{sa}^2\right)^2}. \tag{B.24}$$

Again, best fit results for the proton and neutron electromagnetic form factor are obtained for $\Lambda_{sa}^2 = 0.871\ \mathrm{GeV}^2$ and $\kappa_{sa} = 0.470$.

B.3 Exchange quark-photon diagram

The explicit expression for the exchange quark-photon diagram contribution is given by

$$J_{\alpha\beta}^\mu(Q^2) = \int_{p_f}\int_{p_i}\Big[\bar\Phi^a(p_f,P_f)D^{aa'}(p_{d+}) \Big[S(p_+)\Gamma_{dq}^{b'}(p_1,p_{d-})\Big[S(q')\Gamma_q^\mu(q',q)S(q)\Big]^T \bar\Gamma^{a'}(p_2,p_{d_+})S(p_-)\Big]_{\alpha\beta} D^{b'b}(p_{d-})\Phi^b(p_i,P_i)\Big]. \tag{B.25}$$

All ingredients for this diagram have been discussed already above.

B.4 Seagull diagram

The diquark amplitude-photon diagram contribution is given explicitly by (the corresponding Feynman diagrams have been shown in Fig. 7 and are partially repeated in more detail in Fig. 8)

$$J_{\alpha\beta}^\mu(Q^2) = \int_{p_f}\int_{p_i}\Big[\bar\Phi^a(p_f,P_f)D^{aa'}(p_{d+}) \Big[S(p_+)M^{\mu,b'}(k_1,p_{d-},Q)S^T(q')\bar\Gamma^{a'}(p_2,p_{d+})S(p_-)\Big]_{\alpha\beta} D^{b'b}(p_{d-})\Phi^b(p_i,P_i)\Big]. \tag{B.26}$$

Here we need consider the vertex of a photon interacting with the diquark amplitudes. Again, these vertices have to

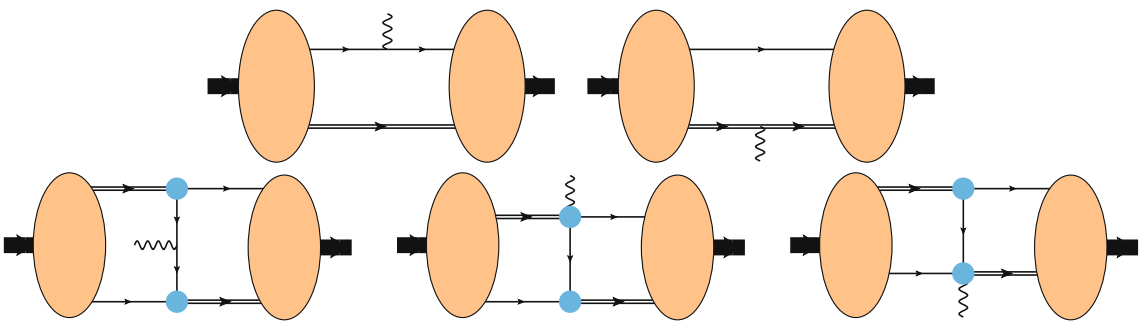

Fig. 7 The diagrams of baryon electromagnetic current operator in the quark-diquark Faddeev equation

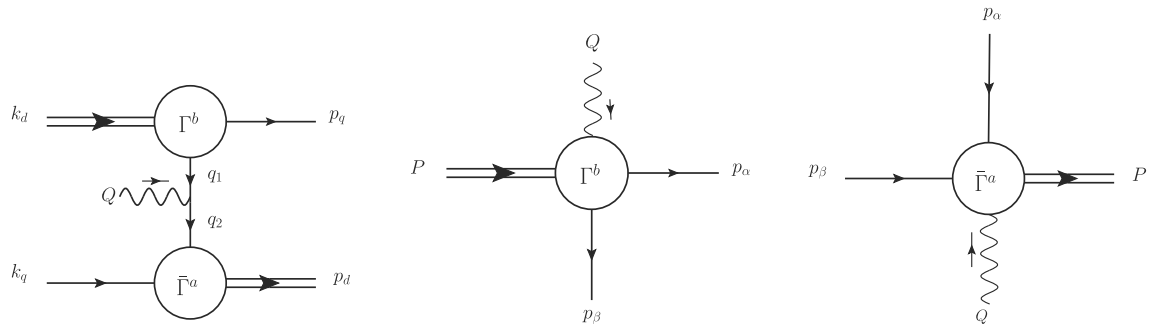

Fig. 8 The Feynman diagrams of exchange (left), seagull (center) and seagullbar (right) in the quark-diquark Faddeev equation

satisfy a Ward–Takahashi identity and we rely again on a Ball–Chiu construction. To this end we only consider the leading term of diquark amplitudes, Eq. (3.7). The gauged quark-diquark vertex is then given by (here we omit the flavor wave functions)

$$M^\mu(p,P,Q) = \left[e_-(p+Q/4)^\mu \triangle^+_{\mathcal{F}} - e_+(p-Q/4)^\mu \triangle^-_{\mathcal{F}}\right] i\gamma_5 C\,, \tag{B.27}$$

$$M^{\mu,\alpha}(p,P,Q) = \left[e_-(p+Q/4)^\mu \triangle^+_{\mathcal{F}} - e_+(p-Q/4)^\mu \triangle^-_{\mathcal{F}}\right] i\gamma^\alpha C\,, \tag{B.28}$$

where

$$\triangle^\pm_{\mathcal{F}} = \frac{\mathcal{F}(p^2_\pm) - \mathcal{F}(p^2)}{p^2_\pm - p^2} = \pm\frac{\mathcal{F}(p^2_\pm) - \mathcal{F}(p^2)}{Q\cdot(q \pm Q/4)}, \tag{B.29}$$

and e_-, e_+ is the charge-flavor factor computed from flavor wave functions. For details, see e.g. Ref. [69].

B.5 Seagull bar diagram

The conjugated diquark amplitude-photon diagram contribution is given by (the sketched Feynman diagram is shown in the right diagram of Fig. 8)

$$J^\mu_{\alpha\beta}(Q^2) = \int_{p_f}\int_{p_i}\Big[\bar{\Phi}^a(p_f,P_f)D^{aa'}(p_{d+}) \Big[S(p_+)\Gamma^{b'}(p_1,p_{d-})S^T(q)\bar{M}^{\mu,a'}(k_2,p_{d+},Q)S(p_-)\Big]_{\alpha\beta} D^{b'b}(p_{d-})\Phi^b(p_i,P_i)\Big]. \tag{B.30}$$

Similar to the diquark amplitude-photon vertex, the gauged conjugated diquark-quark vertex satisfies the following relation with the gauged quark-diquark vertex

$$\bar{M}^\mu(q,P,Q) = -C(M^\mu)^T(-q,-P,Q)C^{-1}\,, \tag{B.31}$$

$$\bar{M}^{\mu,\alpha}(q,P,Q) = C(M^{\mu,\alpha})^T(-q,-P,Q)C^{-1}\,. \tag{B.32}$$

They are given by

$$\bar{M}^\mu(p,P,Q) = \left[e_-(p-Q/4)^\mu \triangle^-_f - e_+(p+Q/4)^\mu \triangle^+_f\right] i\gamma_5 C\,, \tag{B.33}$$

$$\bar{M}^{\mu,\alpha}(p,P,Q) = \left[e_-(p-Q/4)^\mu \triangle^-_f - e_+(p+Q/4)^\mu \triangle^+_f\right] i\gamma^\alpha C\,. \tag{B.34}$$

B.6 Results for the nucleon electromagnetic form factors

In the previous subsections, we summarised the (well-known) framework for the calculation of electromagnetic form factors in the quark-diquark approach. In this framework parameters appear, which have to be fitted to experimental input. To this end we first calculated the nucleon electromagnetic form factors and determined values for the parameters by a best fit to the available experimental data. For simplicity, we selected the empirical fit from experimental data in Ref. [71] as basis for our experimental input.[3] Our objective was to fit the data within the photon momentum range of $Q^2 \sim [1,2]\,\mathrm{GeV}^2$ in order to determine the most optimal parameters. This specific range was chosen for two reasons. First, Due to the absence of explicit meson cloud effects in the current formulation of the quark-diquark Faddeev framework, we cannot expect to perfectly describe nucleons, particularly neutrons, in the infrared momentum range. Second, in the ultraviolet momentum range perturbative logarithmic running sets in, which has never been implemented in the quark-diquark model for simplicity. Hence, our quark-diquark Faddeev approach is aptly suited for intermediate momentum range physics, which is why we specifically opted for $Q^2 \sim [1,2]\,\mathrm{GeV}^2$.

[3] We explicitly checked that fits to more modern representations of the data such as the ones given in Ref. [72] do not change our results materially. We expect this to be also the case for the parametrisation given in the very recent work Ref. [73].

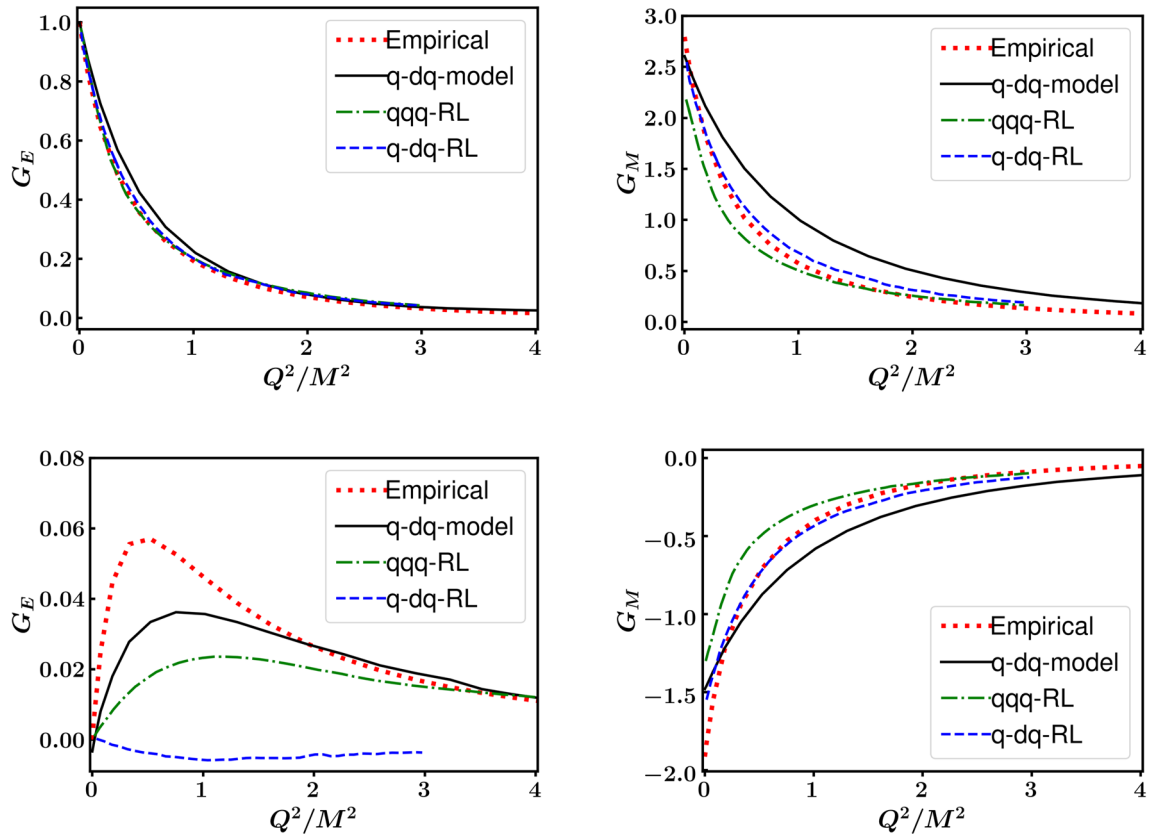

Fig. 9 The comparison of the electric form factor G_E (left) and magnetic form factor G_M (right) of proton (top) and neutron (bottom) which are calculated from quark-diquark Faddeev approach in this work (black solid lines, 'q-dq-model'), the three-body Faddeev approach (green dash-dotted lines, 'qqq-RL') using an effective running coupling in rainbow-ladder ('RL') approximation [40] and the quark-diquark Faddeev approach using the same effective running coupling (blue lines, 'q-dq-RL') [69]. The empirical data (red dotted line) are adapted from [71]

Our results for the electric and magnetic form factors of the proton and the neutron are shown in Fig. 9 ('q-dq-model') together with results from a quark-diquark Faddeev approach using an effective quark-gluon interaction in rainbow-ladder approximation ('q-dq-RL') [69], results from the three-body Faddeev approach using the same effective interaction ('qqq-RL') [40] and empirical fitted results from [71]. The spread in the different DSE/BSE approaches reflect overall systematic uncertainties which are most prominent in the neutron electric form factors but also significant in all other form factors. These uncertainties at small momenta are related to the omission of meson cloud effects. These effects are non-universal and may have a different quantitative impact in different truncation schemes. Their systematic inclusion in the DSE/BSE framework has been explored in a series of works both at zero and finite temperature, see e.g. [59,74–76] and references therein.

In general we observe that for magnetic form factors the decreasing rates are always slower in the quark-diquark picture than in the three-body picture in both proton and neutron cases. This may be due a clustering effect in diquarks which reduces the 'magnetic size' of the nucleon. In contrast to the quark-diquark model discussed in Ref. [38] we have optimized our parameters to best possible match the electric form factor of the neutron rather than the magnetic form factors, as can be seen from the lower panel of Fig. 9. On the flip side we have to live with somewhat too hard magnetic form factors as compared to the empirical curve and the other

Table 5 The best fitting parameters of the elastic electromagnetic form factors of Λ- and Σ- baryon states using Eq.(C.1). Here m_{dq} means the mass parameter of diquarks

		G_E			G_M		
		$95\%m_{dq}$	m_{dq}	$105\%m_{dq}$	$95\%m_{dq}$	m_{dq}	$105\%m_{dq}$
Λ	n_0	0	0	0	−0.393	−0.388	−0.393
	n_1	−0.158	−0.167	−0.229	−0.717	−0.667	−0.451
	d_1	0.944	1.002	1.831	2.544	2.373	1.722
	d_2	0.578	0.525	0.397	0.444	0.412	0.288
	d_3	0.285	0.309	0.480	0.224	0.202	0.135
Σ^+	n_0	1	1	1	2.602	2.465	2.243
	n_1	−0.238	−0.244	−0.243	4.930	19.185	69.491
	d_1	1.690	1.800	1.916	3.300	9.386	33.030
	d_2	0.921	0.929	0.942	2.774	10.384	37.326
	d_3	0.195	0.134	0.108	0.868	3.359	12.808
Σ^0	n_0	0	0	0	0.678	0.658	0.582
	n_1	−0.201	−0.236	−0.272	0.059	10.071	47.353
	d_1	0.916	1.297	1.675	1.299	17.416	80.891
	d_2	0.972	1.019	1.048	0.385	16.899	86.352
	d_3	0.094	0.148	0.214	0.044	5.437	23.572
Σ^-	n_0	−1	−1	−1	−1.250	−1.159	−1.039
	n_1	−1.612	−0.348	−0.245	−4.150	−0.722	−36.272
	d_1	3.111	1.894	1.865	4.913	2.187	37.664
	d_2	2.705	0.897	0.701	5.150	1.343	47.223
	d_3	0.981	0.265	0.223	2.096	0.429	21.592

BSE-approaches. This has to be kept in mind, when predicting form factors of strange baryons and is discussed again in the main par of this work.

C Fitting parameters of the electromagnetic form factors

In Table 5 we provide results for fitting our numerical results for the electromagnetic form factors of Λ and Σ with the fit function

$$G(Q^2) = \frac{n_0 + n_1 Q^2}{1 + d_1 Q^2 + d_2 Q^4 + d_3 Q^6}. \tag{C.1}$$

in analogy to what has been done in Ref. [15].

References

1. Jozef Dudek et al., Physics opportunities with the 12 gev upgrade at jefferson lab. Eur. Phys. J. A **48**, 187 (2012)
2. J. Adamczewski-Musch et al., Production and electromagnetic decay of hyperons: a feasibility study with hades as a phase-0 experiment at fair. Eur. Phys. J. A **57**(4), 138 (2021)
3. L. Tiator, D. Drechsel, S.S. Kamalov, M. Vanderhaeghen, Electromagnetic excitation of nucleon resonances. Eur. Phys. J. Spec. Top. **198**(1), 141 (2011)
4. I.G. Aznauryan, V.D. Burkert, Electroexcitation of nucleon resonances. Prog. Part. Nucl. Phys. **67**(1), 1–54 (2012)
5. G. Eichmann, H. Sanchis-Alepuz, R. Williams, R. Alkofer, C.S. Fischer, Baryons as relativistic three-quark bound states. Prog. Part. Nucl. Phys. **91**, 1–100 (2016)
6. R. Lalik, Status and perspectives of hyperon production and electromagnetic decays with hades at fair. J. Phys. Conf. Ser. **1137**(1), 012057 (2019)
7. G. Ramalho, D. Jido, K. Tsushima, Valence quark and meson cloud contributions for the gamma* lambda -> lambda* and gamma* sigma0 -> lambda* reactions. Phys. Rev. D **85**, 093014 (2012)
8. J. Haidenbauer, U.G. Meißner, The electromagnetic form factors of the λ in the timelike region. Phys. Lett. B **761**, 456–461 (2016)
9. Y. Yang, L. Zhun, The electromagnetic form factors of λ hyperon in $e^+e^- \to \lambda\bar{\Lambda}$. Mod. Phys. Lett. A **33**(22), 1850133 (2018)
10. X. Cao, J.-P. Dai, Y.-P. Xie, Vector mesons and electromagnetic form factor of the λ hyperon. Phys. Rev. D **98**(9), 094006 (2018)
11. Y. Yang, D.-Y. Chen, L. Zhun, Electromagnetic form factors of λ hyperon in the vector meson dominance model. Phys. Rev. D **100**(7), 073007 (2019)
12. G. Ramalho, J.P.B.C. De Melo, K. Tsushima, Octet baryon electromagnetic form factor double ratios $(g_e^*/g_m^*)/(g_e/g_m)$ in a nuclear medium. Phys. Rev. D **100**(1), 014030 (2019)
13. CSSM and QCDSF/UKQCD Collaborations, P.E. Shanahan, R. Horsley, Y. Nakamura, D. Pleiter, P.E.L. Rakow, G. Schierholz, H. Stüben, A.W. Thomas, R.D. Young, J.M. Zanotti, Magnetic form factors of the octet baryons from lattice qcd and chiral extrapolation. Phys. Rev. D **89**(7), 074511 (2014)
14. CSSM and QCDSF/UKQCD Collaborations, P.E. Shanahan, R. Horsley, Y. Nakamura, D. Pleiter, P.E.L. Rakow, G. Schierholz, H. Stüben, A.W. Thomas, R.D. Young, J.M. Zanotti, Electric form fac-

tors of the octet baryons from lattice qcd and chiral extrapolation. Phys. Rev. D **90**(3), 034502 (2014)
15. H. Sanchis-Alepuz, C.S. Fischer, Hyperon elastic electromagnetic form factors in the space-like momentum region. Eur. Phys. J. A **52**(2), 34 (2016)
16. H. Sanchis-Alepuz, R. Alkofer, C.S. Fischer, Electromagnetic transition form factors of baryons in the space-like momentum region. Eur. Phys. J. A **54**(3), 41 (2018)
17. B. Kubis, U.G. Meissner, Baryon form-factors in chiral perturbation theory. Eur. Phys. J. C **18**(FZJ–IKP–TH–2000–25), 747–756 (2001)
18. G. Ramalho, K. Tsushima, Covariant spectator quark model description of the $\gamma^{(*)}\lambda \to \sigma^0$ transition. Phys. Rev. D **86**, 114030 (2012)
19. Z.-Y. Li, J.-J. Xie, Electromagnetic form factors of $\Sigma+$ and $\Sigma-$ in the vector-meson dominance model. Commun. Theor. Phys. **73**(5), 055201 (2021)
20. B. Yan, C. Chen, J.-J. Xie, Σ and Ξ electromagnetic form factors in the extended vector meson dominance model. Phys. Rev. D **107**(7), 076008 (2023)
21. Y.-L. Liu, M.-Q. Huang, Electromagnetic form factors of the lambda and sigma baryons in an alternative baryonic current approach. Phys. Rev. D **79**, 114031 (2009)
22. C. Granados, S. Leupold, E. Perotti, The electromagnetic sigma-to-lambda hyperon transition form factors at low energies. Eur. Phys. J. A **53**(6), 117 (2017)
23. O. Junker, S. Leupold, E. Perotti, T. Vitos, Electromagnetic form factors of the transition from the spin-3/2 σ to the λ hyperon. Phys. Rev. C **101**(1), 015206 (2020)
24. Y.-H. Lin, H.-W. Hammer, U.-G. Meißner, Dispersion-theoretical analysis of the electromagnetic form factors of the Λ hyperon. Eur. Phys. J. C **82**(12), 1091 (2022)
25. Y.-H. Lin, H.-W. Hammer, U. Meißner, The electromagnetic sigma-to-lambda transition form factors with coupled-channel effects in the space-like region. Eur. Phys. J. A **59**(3), 54 (2023)
26. S. Dobbs, K.K. Seth, A. Tomaradze, T. Xiao, G. Bonvicini, Hyperon form factors and diquark correlations. Phys. Rev. D **96**(9), 092004 (2017)
27. M. Oettel, G. Hellstern, R. Alkofer, H. Reinhardt, Octet and decuplet baryons in a covariant and confining diquark - quark model. Phys. Rev. C **58**, 2459–2477 (1998)
28. J.C.R. Bloch, C.D. Roberts, S.M. Schmidt, A. Bender, M.R. Frank, Nucleon form factors and a nonpointlike diquark. Phys. Rev. C **60**(6), 062201 (1999)
29. MYu. Barabanov et al., Diquark correlations in hadron physics: origin, impact and evidence. Prog. Part. Nucl. Phys. **116**, 103835 (2021)
30. G. Hellstern, R. Alkofer, M. Oettel, H. Reinhardt, Nucleon form factors in a covariant diquark-quark model. Nucl. Phys. A **627**(4), 679–709 (1997)
31. D. Nicmorus, G. Eichmann, A. Krassnigg, R. Alkofer, Delta-baryon mass in a covariant Faddeev approach. Phys. Rev. D **80**(5), 054028 (2009)
32. G. Eichmann, C.S. Fischer, H. Sanchis-Alepuz, Light baryons and their excitations. Phys. Rev. D **94**(9), 094033 (2016)
33. G. Eichmann, C.S. Fischer, Baryon structure and reactions from Dyson–Schwinger equations. Few-Body Syst. **60**(1), 2 (2018)
34. C. Chen, B. El-Bennich, C.D. Roberts, S.M. Schmidt, J. Segovia, Shaolong Wan, Structure of the nucleon's low-lying excitations. Phys. Rev. D **97**(3), 034016 (2018)
35. C. Chen, G.I. Krein, C.D. Roberts, S.M. Schmidt, J. Segovia, Spectrum and structure of octet and decuplet baryons and their positive-parity excitations. Phys. Rev. D **100**(5), 054009 (2019)
36. L. Liu, C. Chen, L. Ya, C.D. Roberts, J. Segovia, Composition of low-lying $J = \frac{3}{2}^{\pm}$ Δ-baryons. Phys. Rev. D **105**(11), 114047 (2022)
37. L. Liu, C. Chen, C.D. Roberts, Wave functions of $(I, J^P) = (\frac{1}{2}, \frac{3}{2}^{\mp})$ baryons. Phys. Rev. D **107**(1), 014002 (2023)
38. I.C. Cloet, G. Eichmann, B. El-Bennich, T. Klahn, C.D. Roberts, Survey of nucleon electromagnetic form factors. Few Body Syst. **46**, 1–36 (2009)
39. D. Nicmorus, G. Eichmann, R. Alkofer, Delta and omega electromagnetic form factors in a Dyson–Schwinger/Bethe–Salpeter approach. Phys. Rev. D **82**, 114017 (2010)
40. G. Eichmann, Nucleon electromagnetic form factors from the covariant Faddeev equation. Phys. Rev. D **84**(1), 014014 (2011)
41. D.J. Wilson, I.C. Cloët, L. Chang, C.D. Roberts, Nucleon and roper electromagnetic elastic and transition form factors. Phys. Rev. C **85**(2), 025205 (2012)
42. G. Eichmann, D. Nicmorus, Nucleon to delta electromagnetic transition in the Dyson-Schwinger approach. Phys. Rev. D **85**(9), 093004 (2012)
43. J. Segovia, I.C. Cloet, C.D. Roberts, S.M. Schmidt, Nucleon and δ elastic and transition form factors. Few Body Syst. **55**, 1185–1222 (2014)
44. J. Segovia, C. Chen, I.C. Cloët, C.D. Roberts, S.M. Schmidt, Shaolong Wan, Elastic and transition form factors of the $\delta(1232)$. Few-Body Syst. **55**(1), 1–33 (2014)
45. L. Ya, C. Chen, Z.-F. Cui, C.D. Roberts, S.M. Schmidt, Jorge Segovia, Hong Shi Zong, Transition form factors: $\gamma^* + p \to \Delta(1232)$, $\Delta(1600)$. Phys. Rev. D **100**(3), 034001 (2019)
46. C. Chen, L. Ya, D. Binosi, C.D. Roberts, J. Rodríguez-Quintero, J. Segovia, Nucleon-to-roper electromagnetic transition form factors at large q^2. Phys. Rev. D **99**(3), 034013 (2019)
47. L.X. Khépani Raya, A.B. Gutiérrez-Guerrero, L. Chang, Z.-F. Cui, L. Ya, Craig D. Roberts, Jorge Segovia, Dynamical diquarks in the $\gamma^{(*)} p \to N(1535)\frac{1}{2}^-$ transition. Eur. Phys. J. A **57**(9), 266 (2021)
48. P. Cheng, F.E. Serna, Z.-Q. Yao, C. Chen, Z.-F. Cui, C.D. Roberts, Contact interaction analysis of octet baryon axial-vector and pseudoscalar form factors. Phys. Rev. D **106**(5), 054031 (2022)
49. C. Chen, C.S. Fischer, C.D. Roberts, J. Segovia, Nucleon axial-vector and pseudoscalar form factors and pcac relations. Phys. Rev. D **105**(9), 094022 (2022)
50. K. Kusaka, G. Piller, A.W. Thomas, A.G. Williams, Deep-inelastic structure functions in a covariant spectator model. Phys. Rev. D **55**(9), 5299–5308 (1997)
51. K.D. Bednar, I.C. Cloët, P.C. Tandy, Nucleon quark distribution functions from the Dyson-Schwinger equations. Phys. Lett. B **782**, 675–681 (2018)
52. L. Chang, F. Gao, C.D. Roberts, Parton distributions of light quarks and antiquarks in the proton. Phys. Lett. B **829**, 137078 (2022)
53. I.C. Cloet, C.D. Roberts, Explanation and prediction of observables using continuum strong qcd. Prog. Part. Nucl. Phys. **77**, 1–69 (2014)
54. H. Sanchis-Alepuz, R. Williams, Recent developments in bound-state calculations using the dyson-schwinger and bethe-salpeter equations. Comput. Phys. Commun. **232**, 1–21 (2018)
55. A.B. Henriques, B.H. Kellett, R.G. Moorhouse, General three spinor wave functions and the relativistic quark model. Ann. Phys. **93**, 125 (1975)
56. G. Eichmann, A. Krassnigg, M. Schwinzerl, R. Alkofer, A covariant view on the nucleons' quark core. Ann. Phys. **323**, 2505–2553 (2008)
57. P.-L. Yin, C. Chen, C.S. Fischer, C.D. Roberts, Δ-Baryon axialvector and pseudoscalar form factors, and associated PCAC relations. Eur. Phys. J. A **59**(7), 163 (2023)
58. J. Bernhardt, C.S. Fischer, From imaginary to real chemical potential qcd with functional methods. Eur. Phys. J. A **59**(8), 181 (2023)

59. H. Sanchis-Alepuz, C.S. Fischer, S. Kubrak, Pion cloud effects on baryon masses. Phys. Lett. B **733**, 151–157 (2014)
60. H. Haberzettl, Gauge invariant theory of pion photoproduction with dressed hadrons. Phys. Rev. C **56**, 2041–2058 (1997)
61. A.N. Kvinikhidze, B. Blankleider, Gauging of equations method. 1. Electromagnetic currents of three distinguishable particles. Phys. Rev. C **60**, 044003 (1999)
62. A.N. Kvinikhidze, B. Blankleider, Gauging of equations methods. 2. Electromagnetic currents of three identical particle. Phys. Rev. C **60**, 044004 (1999)
63. M. Oettel, M. Pichowsky, L. von Smekal, Current conservation in the covariant quark diquark model of the nucleon. Eur. Phys. J. A **8**, 251–281 (2000)
64. M. Oettel, R. Alkofer, L. von Smekal, Nucleon properties in the covariant quark diquark model. Eur. Phys. J. A **8**, 553–566 (2000)
65. R.L. Workman et al., Review of particle physics. PTEP **2022**, 083C01 (2022)
66. H.-W. Lin, K. Orginos, Strange baryon electromagnetic form factors and su(3) flavor symmetry breaking. Phys. Rev. D **79**(JLAB–THY–08–928), 074507 (2009)
67. S. Boinepalli, D.B. Leinweber, A.G. Williams, J.M. Zanotti, J.B. Zhang, Precision electromagnetic structure of octet baryons in the chiral regime. Phys. Rev. D **74**, 093005 (2006)
68. G. Eichmann, C.S. Fischer, Nucleon axial and pseudoscalar form factors from the covariant faddeev equation. Eur. Phys. J. A **48**, 9 (2012)
69. G. Eichmann, *Hadron properties from QCD bound-state equations*. PhD thesis, Graz U (2009)
70. M.S. Bhagwat, P. Maris, Vector meson form factors and their quark-mass dependence. Phys. Rev. C **77**, 025203 (2008)
71. J.J. Kelly, Simple parametrization of nucleon form factors. Phys. Rev. C **70**, 068202 (2004)
72. Z. Ye, J. Arrington, R.J. Hill, G. Lee, Proton and neutron electromagnetic form factors and uncertainties. Phys. Lett. B **777**, 8–15 (2018)
73. Y.-H. Lin, H.-W. Hammer, U.-G. Meißner, New Insights into the Nucleon's Electromagnetic Structure. Phys. Rev. Lett. **128**(5), 052002 (2022)
74. C.S. Fischer, D. Nickel, J. Wambach, Hadronic unquenching effects in the quark propagator. Phys. Rev. D **76**, 094009 (2007)
75. C.S. Fischer, R. Williams, Beyond the rainbow: effects from pion back-coupling. Phys. Rev. D **78**, 074006 (2008)
76. P.J. Gunkel, C.S. Fischer, Locating the critical endpoint of qcd: Mesonic backcoupling effects. Phys. Rev. D **104**(5), 054022 (2021)